Modification and evaluation of a FRF-based model updating method for identification of viscoelastic constitutive models for a nonlinear polyurethane adhesive in a bonded joint

Mehdi F. Najib [a], Ali S. Nobari [b]

[a] Aerospace Engineering Department, Amirkabir University of Technology, 424 Hafez Av., Tehran, Iran. fathalizadeh@aut.ac.ir, mfathalizadeh@gmail.com

[b] Corresponding author, Aerospace Engineering Department and Centre of Excellence in Computational Aerospace Engineering, Amirkabir University of Technology, 424 Hafez Av., Tehran, Iran. *Tel.*: +98 21 64543208. a.salehzadeh-nobari@imperial.ac.uk, sal1358@aut.ac.ir

Abstract

In this study, a Frequency Response Function (FRF) -based model updating method, was modified for the purpose of the identification of viscoelastic constitutive models. A steel beam, bonded to a heavy rigid steel block by a layer of Sikaflex-252 polyurethane adhesive, was employed as the test setup. Using the concept of Optimum Equivalent Linear FRF (OELF), accelerance FRFs were measured at different random excitation levels which demonstrated the nonlinear behavior of the adhesive. Using a finite element model, the sensitivity analysis showed that the selected FRFs are more sensitive to the storage and loss moduli of the adhesive near the resonances. Therefore, firstly, both of the storage and loss moduli were identified near each resonance separately and the results have been compared with the results based on Inverse Eigen-sensitivity Method (IEM). In continuation, five viscoelastic constitutive models were utilized and identified to characterize the dynamic mechanical properties of the adhesive at different excitation levels. Applying the identified models, the correlation between the FRFs of the FE models and the experimental ones were tested. The results show that amongst the identified models, The Standard Linear Solid (SLS) model in parallel with a viscous or constant structural damper (stiffness proportional) results in better correlation with experiments. Increasing the excitation level, the storage modulus of the adhesive decreases, whereas the loss modulus increases, especially at high frequencies.

Keywords

Polyurethane (A); Elastic modulus (D); Mechanical properties of adhesives (D); Viscoelasticity (D).

1. Introduction*

Nowadays, there are continually growing trends toward application of polyurethane adhesives in many different industries such as wind turbines, construction, automotive and transportation. This type of adhesives requires fewer curing steps than epoxies, resulting in reduced production costs. Some of the other advantages are fatigue resistance, crack retardation and good damping characteristics. So, establishing new techniques to build and tune the Finite Element (FE) models for simulation of the static and dynamic behavior of structures with adhesively bonded joints is an increasing need. He [1] reviewed some of the published work until 2010, relating to the FE analysis of the adhesively bonded joints, in terms of static loading analysis, environmental behaviors, fatigue loading analysis and dynamic characteristics of the adhesively bonded joints.

In response to dynamic loading, most of adhesives demonstrate viscoelastic behavior that may depend on temperature, excitation frequency, excitation amplitude, pre-stress and humidity. Therefore, definition of the viscoelastic constitutive model has a crucial effect on the accuracy of the FE model of an adhesively bonded joint. The viscoelastic constitutive models (viscoelastic characteristics) are not readily available through manufacturers' data sheets in which usually static, linear characteristics of the adhesives are provided. Consequently, identification of viscoelastic constitutive models for the adhesives is an inspiring research topic in dynamic FE modelling of adhesively bonded joints.

There are extensive studies, with different methods, on the identification of viscoelastic constitutive models of the adhesives. Recently, Najib and Nobari [2] classified these methods into two categories, namely, direct and inverse identification methods, that is repeated here briefly with some instances.

In the direct methods, for a prepared test specimen, dynamic test data are obtained using a selected experimental procedure, for instances, dynamic mechanical thermal analysis (DMTA) (Barruetabena et al. [3]) or resonance testing (Maheri and Adams [4]). These

---

Abbreviations:
ACC: Amplitude Correlation Coefficient
EMA: Experimental Modal Analysis
FE: Finite Element
FRAC: Frequency Response Assurance Criterion
FRF: Frequency Response Function
IEM: Inverse Eigen-sensitivity Method
OELF: Optimum Equivalent Linear FRF
RFM: Response Function Method
SCC: Shape Correlation Coefficient
SLS: Standard Linear Solid model

dynamic data can be converted directly to the dynamic stress-strain data or equivalently to the dynamic modulus at a specific frequency or strain rate. Over a frequency range, the parameters of a viscoelastic model can be obtained by means of curve fitting.

In the category of inverse methods the main point is that the measured dynamic data cannot be converted directly to the dynamic stress-strain data in the adhesive region of the specimen. So, an inverse problem solving is preferable, even inevitable. The methods based on the FE model updating are examples of inverse methods [2],[5],[6],[7].

A recent instance of the methods based on the FE mode updating is the work of Najib and Nobari [2] in which they modified a model updating method based on Frequency Response Function (FRF), referred to as the Response Function Method (RFM), for identification of the parameters of the viscoelastic constitutive model. For a steel beam bonded to a heavy rigid steel block by a layer of adhesive, they measured the accelerance FRFs at different excitation levels, using the concept of Optimum Equivalent Linear FRF (OELF) [14] and identified the parameters of the nonlinear viscoelastic constitutive model. They validated the identified nonlinear viscoelastic model through correlation tests between the FRFs of the updated FE model and the experimental ones.

In this paper, the method developed in [2] will be implemented on 5 different viscoelastic models, in order to identify their parameters and to see which one of the models gives the best prediction of the behavior of the adhesive in question. In this respect, for a beam bonded to a rigid support via a layer of elastic adhesive, the accelerance FRFs were measured experimentally, using the concept of Optimum Equivalent Linear FRF (OELF). These FRFs were used to update the FE model of the bonded beam. The results will be compared with the ones obtained based on IEM. Also, the nonlinearity effects, attributable to the excitation level, will be examined.

2. Formulation of RFM

For the first time, the RFM was proposed by Lin and Ewins [8]. The reader is referred to Najib and Nobari [2] for a brief introduction and to Imregun et al. [9] and Visser [10] for more details and computational aspects. The updating equation that was used in this study is [2]:

$$-\omega^2 H_{A_{ij}}(\omega) - H'_{X_{ij}}(\omega) = \mathbf{H}^{\mathrm{T}}_{A\,i}(\omega)\Delta\mathbf{Z}(\omega)\mathbf{H}'_{X\,j}(\omega) \tag{1}$$

where ω is the circular frequency in (rad/sec), $H_{A_{ij}}$ is the element in *i*-th row and *j*-th column of the analytical receptance matrix ($\mathbf{H}_A$), $H'_{X_{ij}}$ is the element in *i*-th row and *j*-th column of the experimental inertance matrix ($\mathbf{H'}_X$), $\mathbf{H}_{A_i}^{\mathrm{T}}$ is the transpose of *i*-th column of the analytical receptance matrix and $\mathbf{H'}_{X_j}(\omega)$ is the *j*-th column of the experimental inertance matrix. $\Delta\mathbf{Z}$ is the dynamic stiffness error matrix, $\Delta\mathbf{Z} = \mathbf{Z}_X - \mathbf{Z}_A$, where $\mathbf{Z}_A$ and $\mathbf{Z}_X$ are the dynamic stiffness matrices of the analytical and experimental models of structure, respectively. In practice, it is impossible to measure complete set of $\mathbf{H'}_{X_j}$ in (1), so the unmeasured FRFs in $\mathbf{H'}_{X_j}$ will be filled with their analytically-derived counterparts [9]. Since this is an approximation, the method will be an iterative scheme and the convergence must be checked at each iteration step [9].

3. Modification of the RFM for viscoelastic material properties identification

This procedure was presented in [2] and here is repeated. In the frequency domain, the Fourier transforms of stress and strain ($\bar{\sigma}$ and $\bar{\varepsilon}$) are related by:

$$E^*(\omega) = \frac{\bar{\sigma}(\omega)}{\bar{\varepsilon}(\omega)} = E'(\omega) + \mathrm{j}E''(\omega) \tag{2}$$

where $\mathrm{j} = \sqrt{-1}$ and E^*, E' and E'' are referred to as dynamic (or complex) modulus, storage modulus and loss modulus, respectively.

The FE model, that contains two different materials, namely, adherend and adhesive, is considered to modify RFM (Eq. (1)) for identification of unknown viscoelastic properties of the adhesive (E' and E''). The material properties of the adherend are known, whereas those for adhesive are unknown except its density. So, the dynamic stiffness matrix of the FE model can be written down as:

$$\mathbf{Z}(\omega) = -\omega^2\mathbf{M} + \mathbf{K}_{\mathrm{adherend}} + \mathrm{j}\omega\mathbf{C}_{\mathrm{adherend}} + \mathrm{j}\mathbf{D}_{\mathrm{adherend}} + \mathbf{K}^*\left(E^*(\omega)\right)_{\mathrm{adhesive}} \tag{3}$$

where **M** is the complete mass matrix and **K**, **C** and **D** with the subscript "adherend" are those parts of global stiffness, viscous damping and structural damping matrix that are related to the elements of adherend portion of the model and are known. $\mathbf{K}^*$ is the complex stiffness matrix of the adhesive part of the model, i.e.:

$$\mathbf{K}^*\left(E^*(\omega)\right)_{\mathrm{adhesive}} = \mathbf{K}'\left(E'(\omega)\right) + \mathrm{j}\mathbf{K}''\left(E''(\omega)\right) \tag{4}$$

$\mathbf{K}'$ and $\mathbf{K}''$ are the only parts of $\mathbf{Z}$ that are related to the E' and E''. So, at a fixed ω, one can write:

$$\Delta\mathbf{Z} = \Delta\mathbf{K}' + \mathrm{j}\Delta\mathbf{K}'' \tag{5}$$

For the solid element used in this study, the element stiffness matrix is a linear function of Young's modulus. So, assuming uniform Young's modulus for the adhesive layer, Eq. (5) becomes:

$$\Delta\mathbf{Z} = \frac{\partial\mathbf{K}'}{\partial E'}\Delta E' + \mathrm{j}\frac{\partial\mathbf{K}''}{\partial E''}\Delta E'' \tag{6}$$

Defining $\mathbf{S}$ as the sensitivity of stiffness matrix,

$$\frac{\partial\mathbf{K}'}{\partial E'} = \frac{\partial\mathbf{K}''}{\partial E''} = \mathbf{S} = \text{constant} \tag{7}$$

Eq. (6) becomes,

$$\Delta\mathbf{Z} = (\Delta E' + \mathrm{j}\Delta E'')\mathbf{S} = \Delta E^{*}\mathbf{S} \tag{8}$$

and by the definition of

$$B_{ij}(\omega) = \frac{-\omega^2 H_{A_{ij}}(\omega) - H'_{X_{ij}}(\omega)}{\mathbf{H}_{A_i}^{\mathrm{T}}(\omega)\mathbf{S}\mathbf{H}'_{X_j}(\omega)} \tag{9}$$

Eq. (1) reduces to

$$\Delta E^{*}(\omega) = B_{ij}(\omega) \tag{10}$$

The Eq. (10) is the modified version of RFM (Eq. (1)) for identification of viscoelastic properties and it is a complex equation, so:

$$\begin{bmatrix}\Delta E'(\omega)\\ \Delta E''(\omega)\end{bmatrix} = \begin{bmatrix}\mathrm{Re}(B_{ij}(\omega))\\ \mathrm{Im}(B_{ij}(\omega))\end{bmatrix} \tag{11}$$

The Eq. (11) can be used to update E' and E'' at each frequency point. Also, one can write down these equations for a range of frequency points and use least square solution to identify

constant values of the E' and E'' over a frequency range. This will be discussed more in the Section 5.

4. Formulation of IEM

After the original work of Fox and Kapoor [11], the formulation of the IEM has been presented by many researchers for instance by Naraghi and Nobari [7] and here is repeated in brief to be compatible with the present paper notation. Using the same notation as in Section 3, the complex eigen-value problem for the FE model can be written as:

$$(\mathbf{K}_{\text{adherend}} + \mathbf{K'}_{\text{adhesive}} + \mathrm{j}\mathbf{K''}_{\text{adhesive}} - \lambda_r \mathbf{M})\{\phi\}_r = 0 \tag{12}$$

where λ_r and $\{\phi\}_r$ are the r-th eigen-value and eigen-vector of the model and $\{\phi\}_r$ is normalized such that

$$\{\phi\}_r^T \mathbf{M} \{\phi\}_r = 1 \tag{13}$$

Differentiating Eq. (12) with respect to the updating variable E' gives

$$\left(\frac{\partial \mathbf{K'}}{\partial E'} - \frac{\partial \lambda_r}{\partial E'}\mathbf{M}\right)\{\phi\}_r + (\mathbf{K}_{\text{adherend}} + \mathbf{K'} + \mathrm{j}\mathbf{K''} - \lambda_r \mathbf{M})\frac{\partial \{\phi\}_r}{\partial E'} = 0 \tag{14}$$

Pre-multiplying Eq. (14) by $\{\phi\}_r^T$, rearranging the terms and using Eq. (7) leads to

$$\frac{\partial \lambda_r}{\partial E'} = \{\phi\}_r^T \frac{\partial \mathbf{K'}}{\partial E'}\{\phi\}_r = \{\phi\}_r^T \mathbf{S} \{\phi\}_r \tag{15}$$

where $\partial \lambda_r / \partial E'$ is the sensitivity of the r-th eigen-value with respect to the updating parameter E'. Using the same procedure the sensitivity of λ_r with respect to E'' is obtained as

$$\frac{\partial \lambda_r}{\partial E''} = \{\phi\}_r^T \mathrm{j} \frac{\partial \mathbf{K''}}{\partial E''}\{\phi\}_r = \{\phi\}_r^T \mathrm{j}\mathbf{S} \{\phi\}_r \tag{16}$$

Using the first order approximation, one can write:

$$\Delta\lambda_r = \frac{\partial \lambda_r}{\partial E'}\Delta E' + \frac{\partial \lambda_r}{\partial E''}\Delta E'' \tag{17}$$

Putting Eq. (15)-(16) into Eq.(17) yields

$$\Delta\lambda_r = \{\phi\}_r^T \mathbf{S}\{\phi\}_r(\Delta E' + \mathrm{j}\Delta E'') = \{\phi\}_r^T \mathbf{S}\{\phi\}_r \Delta E^* \tag{18}$$

Considering

$$\Delta\lambda_r = \lambda_r^X - \lambda_r^A \tag{19}$$

where λ_r^A is the *r*-th eigen-value of the FE model and λ_r^X is its experimental counterpart, the updating equation for IEM is obtained as

$$\Delta E^* = \frac{\lambda_r^X - \lambda_r^A}{\{\phi\}_r^T \mathbf{S}\{\phi\}_r} \tag{20}$$

Eq. (20) is a complex equation and can be used to update E^* iteratively, at each measured eigen-value separately.

5. Constitutive model in the frequency domain

Five models are selected in this study to represent the viscoelastic behavior in the frequency range of interest (Fig. 1).

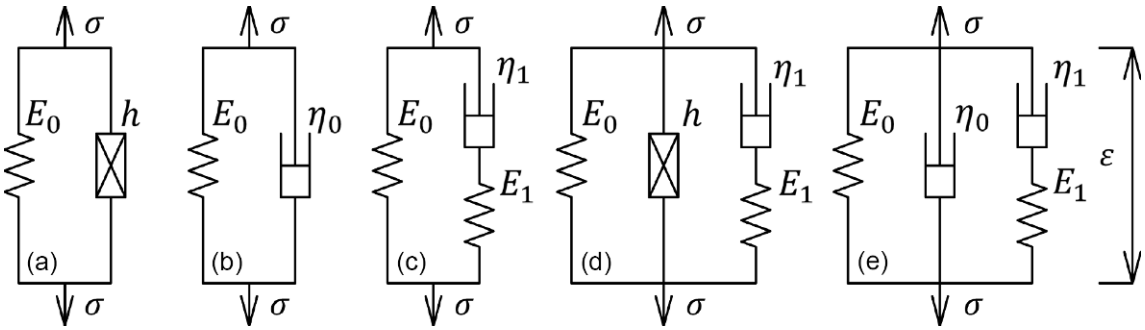

Fig. 1. Examined viscoelastic models. (a)- (e) Model 1-5.

Model 1 (Fig. 1a) is a model with two parameters (E_0 and h) and consists of a Hookean spring in parallel with a structural damping unit. So,

$$E^*(\omega) = E_0 + \mathrm{j}h \tag{21}$$

Comparing Eq. (21) with Eq. (2) the following relations are obtained for storage and loss moduli in term of parameters of Model 1:

$$\begin{matrix} E'(\omega) = E_0 \\ E''(\omega) = h \end{matrix} \tag{22}$$

and

$$\begin{bmatrix} \Delta E'(\omega) \\ \Delta E''(\omega) \end{bmatrix} = \begin{bmatrix} \Delta E_0 \\ \Delta h \end{bmatrix} \tag{23}$$

Inserting Eq. (23) into Eq. (11) it is obtained that

$$\begin{bmatrix} \Delta E_0 \\ \Delta h \end{bmatrix} = \begin{bmatrix} \mathrm{Re}(B_{ij}(\omega)) \\ \mathrm{Im}(B_{ij}(\omega)) \end{bmatrix} \tag{24}$$

Model 2 is the Kelvin–Voigt model, also known as the Voigt model. It consists of a Newtonian damper and Hookean elastic spring connected in parallel, as shown in (Fig. 1b) and has two parameters (E_0 and η_0). So,

$$E^*(\omega) = E_0 + \mathrm{j}\omega\eta_0 \tag{25}$$

and Eq. (11) becomes

$$\begin{bmatrix} 1 & 0 \\ 0 & \omega \end{bmatrix} \begin{bmatrix} \Delta E_0 \\ \Delta \eta_0 \end{bmatrix} = \begin{bmatrix} \mathrm{Re}(B_{ij}(\omega)) \\ \mathrm{Im}(B_{ij}(\omega)) \end{bmatrix} \tag{26}$$

Model 3 (Fig. 1c) is the SLS model which has three parameters (E_0, E_1 and η_1) and consists of a classical Maxwell model in parallel with a Hookean spring unit. After some mathematical manipulation one can obtain the dynamic modulus for the SLS model, as follows:

$$E^*(\omega) = E_0 + \frac{\mathrm{j}\omega E_1 \eta_1}{E_1 + \mathrm{j}\omega\eta_1} \tag{27}$$

Comparing Eq. (27) with Eq. (2) the following relations are obtained for storage and loss moduli in term of parameters of SLS model:

$$\begin{matrix} E'(\omega) = E_0 + \dfrac{\omega^2 E_1 \eta_1^2}{E_1^2 + \omega^2 \eta_1^2} \\ E''(\omega) = \dfrac{\omega E_1^2 \eta_1}{E_1^2 + \omega^2 \eta_1^2} \end{matrix} \tag{28}$$

Using the first order approximation, one can write:

$$\Delta E' \simeq \frac{\partial E'}{\partial E_0}\Delta E_0 + \frac{\partial E'}{\partial E_1}\Delta E_1 + \frac{\partial E'}{\partial \eta_1}\Delta \eta_1 \tag{29}$$

$$\Delta E'' \simeq \frac{\partial E''}{\partial E_0}\Delta E_0 + \frac{\partial E''}{\partial E_1}\Delta E_1 + \frac{\partial E''}{\partial \eta_1}\Delta \eta_1 \tag{30}$$

Inserting Eq. (29) and (30) into Eq. (11) it is obtained that:

$$\begin{bmatrix} \frac{\partial E'}{\partial E_0} & \frac{\partial E'}{\partial E_1} & \frac{\partial E'}{\partial \eta_1} \\ \frac{\partial E''}{\partial E_0} & \frac{\partial E''}{\partial E_1} & \frac{\partial E''}{\partial \eta_1} \end{bmatrix} \begin{bmatrix} \Delta E_0 \\ \Delta E_1 \\ \Delta \eta_1 \end{bmatrix} = \begin{bmatrix} \mathrm{Re}(B_{ij}(\omega)) \\ \mathrm{Im}(B_{ij}(\omega)) \end{bmatrix} \tag{31}$$

Differentiating Eq. (28) with respect to design parameters, Eq. (31) becomes

$$\begin{bmatrix} 1 & \frac{\omega^4\eta_1^4 - \omega^2 E_1^2\eta_1^2}{(E_1^2+\omega^2\eta_1^2)^2} & \frac{2\omega^2 E_1^3\eta_1}{(E_1^2+\omega^2\eta_1^2)^2} \\ 0 & \frac{2\omega^3 E_1\eta_1^3}{(E_1^2+\omega^2\eta_1^2)^2} & \frac{E_1^2\omega(E_1^2-\omega^2\eta_1^2)}{(E_1^2+\omega^2\eta_1^2)^2} \end{bmatrix} \begin{bmatrix} \Delta E_0 \\ \Delta E_1 \\ \Delta \eta_1 \end{bmatrix} = \begin{bmatrix} \mathrm{Re}(B_{ij}(\omega)) \\ \mathrm{Im}(B_{ij}(\omega)) \end{bmatrix} \tag{32}$$

Model 4 (Fig. 1d) consists of Model 2 in parallel with a constant structural damping unit. This model has four parameters (E_0, h, E_1 and η_1). The dynamic modulus for the Model 4 is as follows:

$$E^*(\omega) = E_0 + \mathrm{j}h + \frac{\mathrm{j}\omega\eta_1 E_1}{E_1 + \mathrm{j}\omega\eta_1} \tag{33}$$

Using the same procedure as for Model 3 Eq. (11) for Model 4 is obtained as:

$$\begin{bmatrix} 1 & 0 & \frac{\omega^4\eta_1^4 - \omega^2 E_1^2\eta_1^2}{(E_1^2+\omega^2\eta_1^2)^2} & \frac{2\omega^2 E_1^3\eta_1}{(E_1^2+\omega^2\eta_1^2)^2} \\ 0 & 1 & \frac{2\omega^3 E_1\eta_1^3}{(E_1^2+\omega^2\eta_1^2)^2} & \frac{E_1^2\omega(E_1^2-\omega^2\eta_1^2)}{(E_1^2+\omega^2\eta_1^2)^2} \end{bmatrix} \begin{bmatrix} \Delta E_0 \\ \Delta h \\ \Delta E_1 \\ \Delta \eta_1 \end{bmatrix} = \begin{bmatrix} \mathrm{Re}(B_{ij}(\omega)) \\ \mathrm{Im}(B_{ij}(\omega)) \end{bmatrix} \tag{34}$$

Model 5 consists of a Maxwell model and a Voigt model connected in parallel, as shown in (Fig. 1e) and has four parameters (E_0, h, E_1 and η_1). The dynamic modulus for the Model 5 is as follows:

$$E^*(\omega) = E_0 + \mathrm{j}\omega\eta_0 + \frac{\mathrm{j}\omega\eta_1 E_1}{E_1 + \mathrm{j}\omega\eta_1} \tag{35}$$

Finally, Eq. (11) for Model 5 is obtained as:

$$\begin{bmatrix} 1 & 0 & \frac{\omega^4\eta_1^4 - \omega^2 E_1^2\eta_1^2}{(E_1^2+\omega^2\eta_1^2)^2} & \frac{2\omega^2 E_1^3\eta_1}{(E_1^2+\omega^2\eta_1^2)^2} \\ 0 & \omega & \frac{2\omega^3 E_1\eta_1^3}{(E_1^2+\omega^2\eta_1^2)^2} & \frac{E_1^2\omega(E_1^2-\omega^2\eta_1^2)}{(E_1^2+\omega^2\eta_1^2)^2} \end{bmatrix} \begin{bmatrix} \Delta E_0 \\ \Delta\eta_0 \\ \Delta E_1 \\ \Delta\eta_1 \end{bmatrix} = \begin{bmatrix} \mathrm{Re}(B_{ij}(\omega)) \\ \mathrm{Im}(B_{ij}(\omega)) \end{bmatrix} \tag{36}$$

Eqs. (24), (26), (32), (34) and (36) can be written down at each frequency point for each measured FRF. Using all of the measured FRFs at all of the selected frequency points, a system of simultaneous equation can be written as:

$$\mathbf{U}_{2N_H N_f \times N_p}\mathbf{P}_{N_p \times 1} = \mathbf{D}_{2N_H N_f \times 1} \tag{37}$$

where, N_f is the number of frequency points, N_H is the number of measured FRFs and N_p is the number of parameters in viscoelastic constitutive model. **P** is the vector of parameter changes and **D** is a known vector and **U** is the global sensitivity matrix relating parameter changes to response changes. Commonly, Eq. (37) is an over-determined system and can be solved using the least-square solution. The Singular Value Decomposition (SVD) approach was utilized to diagnose the rank-deficient systems.

6. FRF correlation tests

FRF correlation tests are used to assess the level of correlation between the measured FRFs and their updated analytical counterparts. As in Najib and Nobari [2], three different correlation criteria are used in this study.

Frequency Response Assurance Criterion (FRAC) [2], [12]:

$$\mathrm{FRAC}(\mathbf{H}_{X_{ij}}, \mathbf{H}_{A_{ij}}) = \frac{\left|\mathbf{H}_{X\,ij}^{\mathrm{H}} \times \mathbf{H}_{A_{ij}}\right|^2}{\left(\mathbf{H}_{X\,ij}^{\mathrm{H}} \times \mathbf{H}_{X_{ij}}\right)\left(\mathbf{H}_{A\,ij}^{\mathrm{H}} \times \mathbf{H}_{A_{ij}}\right)} \tag{38}$$

where the superscript H is the conjugate transpose operator, $\mathbf{H}_{X_{ij}}$ is a N_f (the number of frequency points) × 1 vector of a measured FRF along the frequency axis for the excitation at the *j*-th DOF and response at the *i*-th DOF and $\mathbf{H}_{A_{ij}}$ is its analytical counterpart. Hereinafter, $\mathrm{FRAC}(\mathbf{H}_{X_{ij}}, \mathbf{H}_{A_{ij}})$ is referred to as FRAC_{ij}.

Shape Correlation Coefficient (SCC) [2], [13]:

$$\chi_s(\omega_k) = \frac{\left|\mathbf{H}_X^{\mathrm{H}}(\omega_k) \times \mathbf{H}_A(\omega_k)\right|^2}{\left(\mathbf{H}_X^{\mathrm{H}}(\omega_k) \times \mathbf{H}_X(\omega_k)\right)\left(\mathbf{H}_A^{\mathrm{H}}(\omega_k) \times \mathbf{H}_A(\omega_k)\right)} \tag{39}$$

where $\mathbf{H}_X(\omega_k)$ and $\mathbf{H}_A(\omega_k)$ are N_H (the number of measured FRFs) × 1 vectors of measured and analytical FRFs at matching excitation/response locations.

Amplitude Correlation Coefficient (ACC) [2], [13]:

$$\chi_a(\omega_k) = \frac{2\left|\mathbf{H}_X^{\mathrm{H}}(\omega_k) \times \mathbf{H}_A(\omega_k)\right|}{\mathbf{H}_X^{\mathrm{H}}(\omega_k) \times \mathbf{H}_X(\omega_k) + \mathbf{H}_A^{\mathrm{H}}(\omega_k) \times \mathbf{H}_A(\omega_k)} \tag{40}$$

7. Sensitivity of FRF

Using the same notation as in Sections 2-03 the sensitivity of receptance FRF matrix with respect to a design parameter (p) can be obtained using

$$\mathbf{HZ} = \mathbf{ZH} = \mathbf{I} \tag{41}$$

as:

$$\frac{\partial \mathbf{H}}{\partial p} = \frac{\partial \mathbf{HI}}{\partial p} = \frac{\partial \mathbf{HZH}}{\partial p} \tag{42}$$

Making differentiation of the Eq. (42), it is obtained that

$$\frac{\partial \mathbf{H}}{\partial p} = \frac{\partial \mathbf{H}}{\partial p}\mathbf{ZH} + \mathbf{H}\frac{\partial \mathbf{Z}}{\partial p}\mathbf{H} + \mathbf{HZ}\frac{\partial \mathbf{H}}{\partial p} \tag{43}$$

Using Eq. (41) again, the sensitivity of **H** can be written down in term of the sensitivity of **Z** matrix as

$$\frac{\partial \mathbf{H}}{\partial p} = -\mathbf{H}\frac{\partial \mathbf{Z}}{\partial p}\mathbf{H} \tag{44}$$

Considering the element in i-th row and j-th column of Eq. (44), one obtains:

$$\frac{\partial H_{ij}}{\partial p} = -\mathbf{H}_i^{\mathrm{T}}\frac{\partial \mathbf{Z}}{\partial p}\mathbf{H}_j \tag{45}$$

where $\mathbf{H}_j$ is the j-th column of the receptance matrix and $\mathbf{H}_i^{\mathrm{T}}$ is its i-th column transpose. For E' and E'' as the design parameters, the sensitivities of an accelerance FRF with respect to storage and loss modulus is obtained as:

$$\frac{\partial H'_{ij}}{\partial E'} = -\mathbf{H}_i^{\mathrm{T}}\mathbf{S}\mathbf{H}'_j \tag{46}$$

$$\frac{\partial H'_{ij}}{\partial E''} = -\mathrm{j}\mathbf{H}_i^{\mathrm{T}}\mathbf{S}\mathbf{H}'_j \tag{47}$$

8. Experimental procedure

The experimental setup is identical to that used in [2]. It consists of a 300 mm×10 mm ×20 mm steel beam (adherend) that is bonded to a heavy rigid steel block by a 50 mm×10 mm ×20 mm adhesive layer (Fig. 2). The adhesive is Sikaflex-252, a one-component polyurethane adhesive, which cures with atmospheric moisture. The four points on the upper surface of the beam that were used as the excitation and response points are shown in Fig. 2.

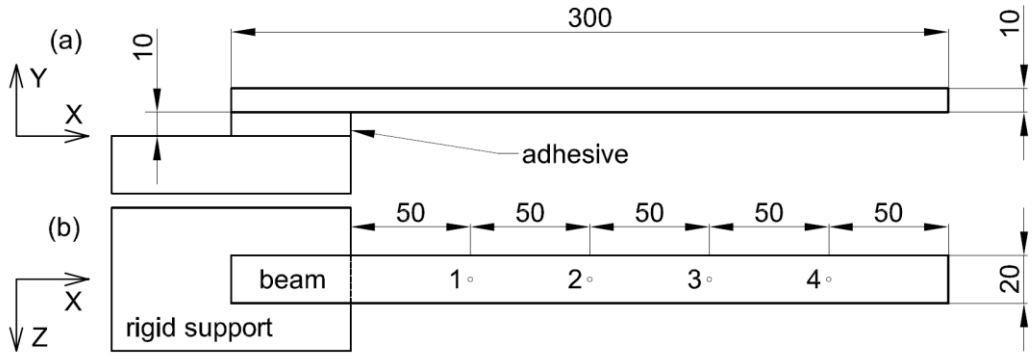

Fig. 2. (a) side view and (b) top view of the bonded beam and the points 1-4 (the dimensions are in mm and the rigid support block is sketched schematically).

The Sikaflex-252 adhesive's specifications can be found in the adhesive product data sheet [15] and the applying procedure was explained by Najib and Nobari [2] and here is avoided for the sake of brevity.

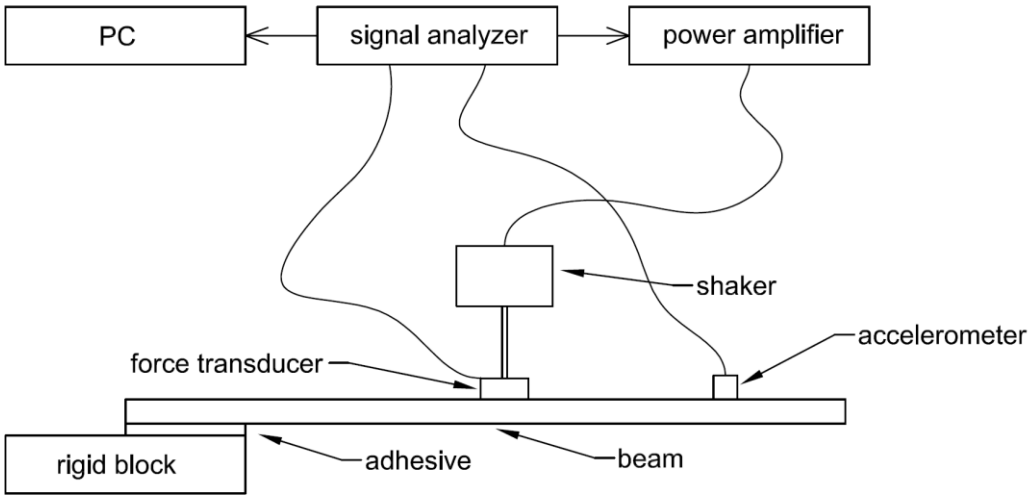

Fig. 3. The test setup.

In order to be able to investigate the effect of excitation level on the identified model, the test has been performed for the two excitation levels. Level 1 and Level 2 which correspond to the zero mean value random signals with 3.3 N and 46.2 N RMS, respectively. The analyzer was set to compute the OELF [2], [14] using:

$$H'_{i2} = \frac{S_{\ddot{y}_i f_2}}{S_{f_2 f_2}} \tag{48}$$

Where, $S_{\ddot{y}_i f_2}$ is the cross-spectrum of the acceleration at the point i (i=1-4) and the excitation force at the point 2 and $S_{f_2 f_2}$ is the auto-spectrum of the excitation force at the point 2.

Fixing the shaker at the point 2, the four accelerance FRFs were measured at the points 1-4 in Y direction using the test setup shown in Fig. 3. The frequency band of measurement was set to be within the 0-500 Hz with 1 Hz resolution. The analyzer was set to make 200 averages to attenuate measurement noise. The amplitudes of measured FRFs are presented in Fig. 4.

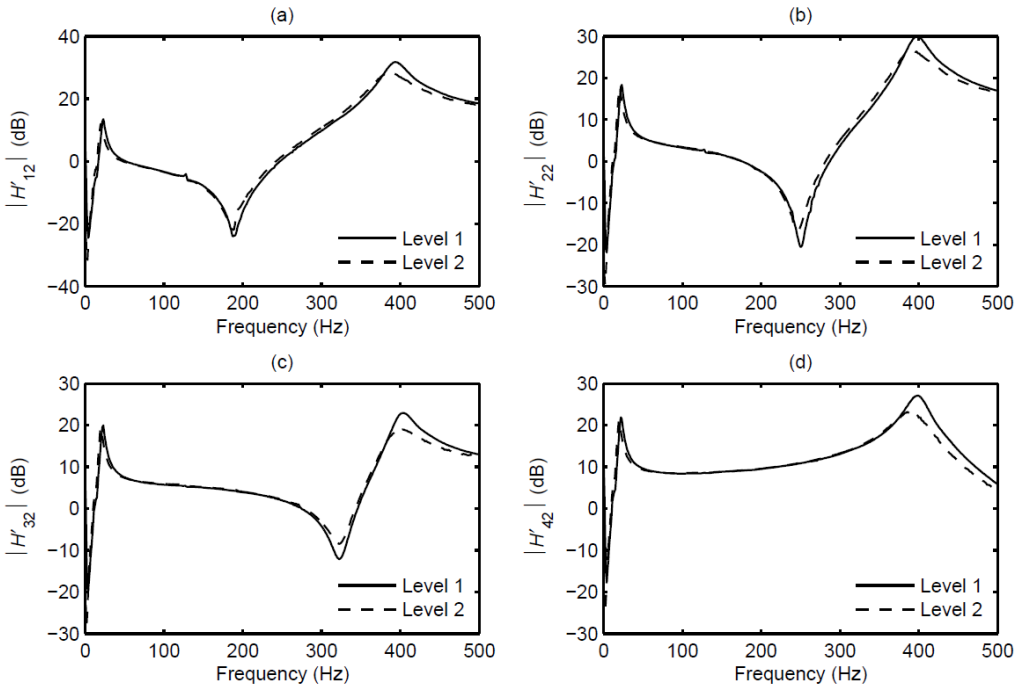

Fig. 4. Amplitude of measured FRFs for the bonded beam at the excitation Levels 1-2.

9. FE models

Using the ANSYS software a FE model was built for the bonded beam using 3D brick SOLID186 elements. This element has 20 nodes, that each node has three translational DOFs in X, Y and Z directions. The following material properties were considered for the beam and adhesive [2], [15].

Beam: density = 7800 kg m^{-3}, Poisson's ratio= 0.3.

Adhesive: density = 1160 kg m^{-3}, Poisson's ratio= 0.44.

A convergence study has been performed to obtain the appropriate mesh size. Four different FE models with uniform element sizes according to Table 1 were tested. The FRF, H_{22}, was obtained from each model, using the viscoelastic Model 1 with the values of E_0 = 6 MPa and h = 1 MPa for the adhesive, which presented in Fig. 5. Comparing the results quantitatively, it was observed that except the Mesh 1, the other meshes have very close FRFs. So, the Mesh 1 is not a converged. Therefore it can be concluded that the mesh size in FE model with Mesh 2 is refined enough for the purpose of adhesive material characterization.

Table 1: Convergence study on the FE model.

Mesh	Element size $X \times Y \times Z$ (mm)	FRAC[a]
1	25×10×20	0.6571
2	12.5×5×10	0.9900
3	8.33×3.33×6.67	0.9985
4	6.25×2.5×5	1

[a] $\mathrm{FRAC} = \mathrm{FRAC}(H_{22}^{\text{Mesh 4}}, H_{22}^{\text{Mesh i}}), i = 1 \ldots 4$

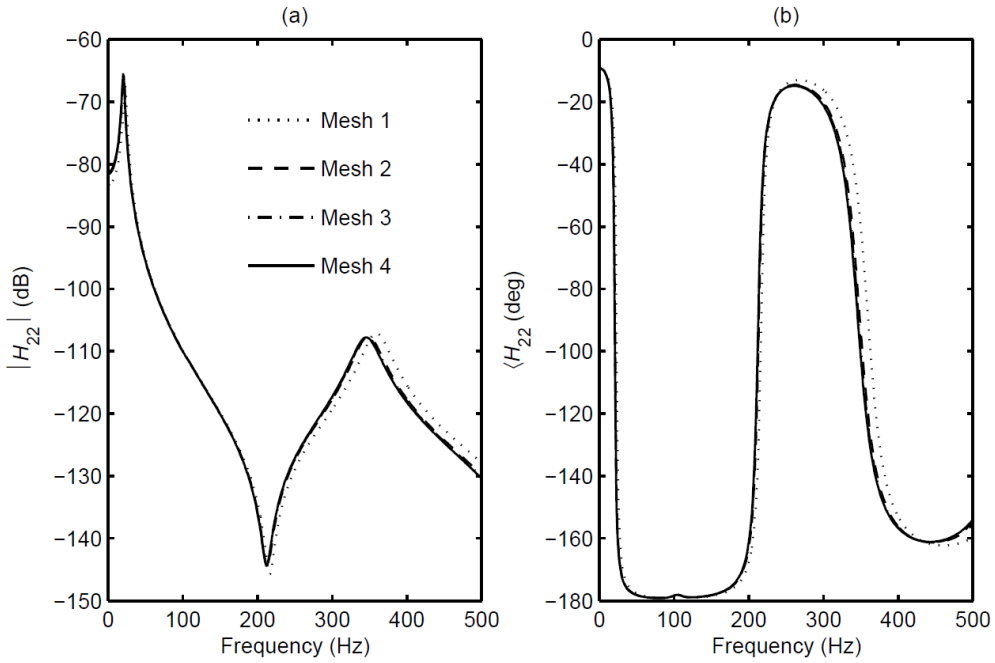

Fig. 5. The amplitude and phase of the H_{22} from FE models with the mesh sizes according to Table 1.

In the FE model, adjacent nodes of the beam and the adhesive on the bonding surface were merged to simulate perfect bonding. All of the nodes on the lower surface of the adhesive layer were constrained to simulate bonding to rigid support. The FE model is shown in Fig. 6.

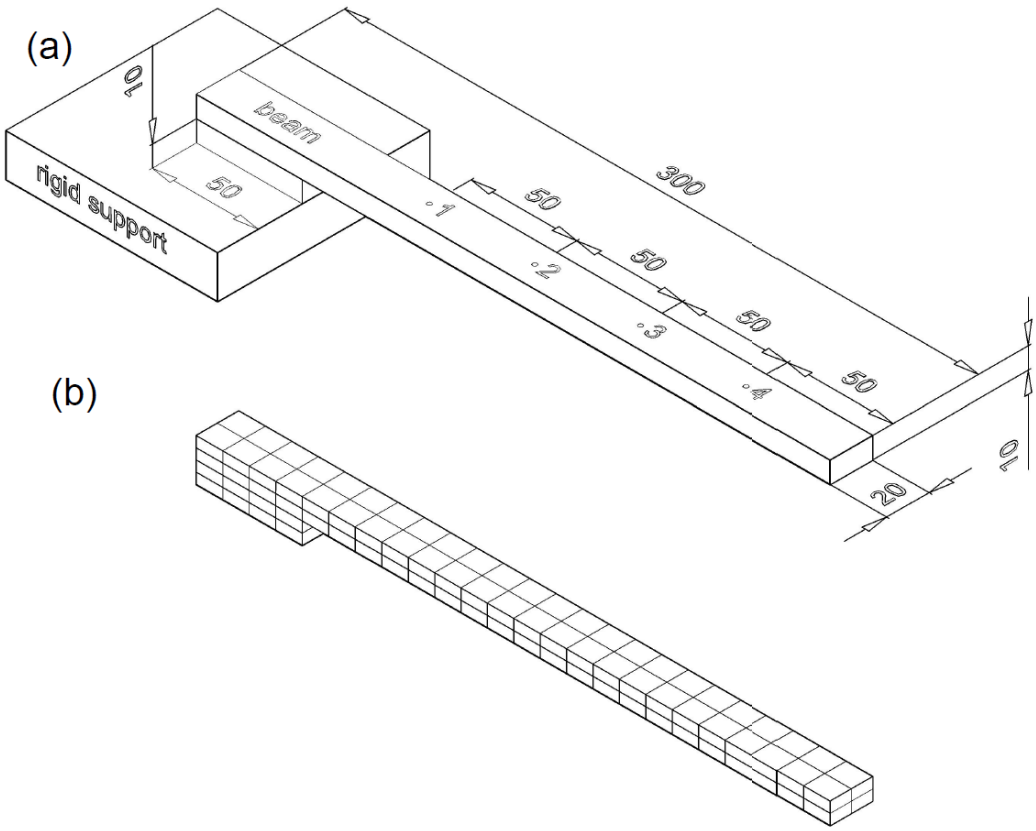

Fig. 6. (a) 3D sketch of the bonded beam (the dimensions are in mm and the rigid support block is sketched schematically), (b) FE mesh.

Once the FE model was built in ANSYS, the global mass matrix and stiffness matrices for the beam and adhesive were exported to separate text files. Using these files and experimentally measured FRF data, a computer program has been coded to rebuild the FE model and assemble the system of Eq. (37) and solve it using SVD method. At each iteration, after solving the system of equations, the necessary parameters changes were obtained and the parameters were updated. If the parameters changes become smaller than pre-specified thresholds, the iteration must be stopped and the parameters would converge to fixed values. Selection of appropriate values for the initial values of the parameters has a crucial effect on the success of updating process.

10. Case study 1: Comparison between the RFM and the IEM

In this case study, the results of the present method will be compared to those obtained based on the IEM (Section 4). In order to ensure that in the bonded beam case, the difference between the analytical and measured FRFs originates only from the adhesive, the FE model of the free-free beam has been updated which yields Young's modulus of 198 GPa for elastic beam [2].

Two distinct and dominant peaks are apparent in the amplitude of measured FRFs. These peaks are far enough from each other that make it feasible to use a single DOF approximation method for the purpose of EMA and extraction of modal parameters. So, the circle-fitting method [16] was utilized to extract modal frequencies and loss factors from the measured FRFs. The results are presented in Table 2.

Table 2: Extracted modal parameters.

Excitation level (N)	Frequency (Hz)	loss factor (-)
3.3	22.26 Hz	0.2044
	394.45 Hz	0.0720
46.2	19.28 Hz	0.2202
	387.33 Hz	0.1121

Using the IEM, the storage and loss moduli were identified at these modes for both levels using Eq. (20), iteratively. Also, Model 1 was assumed in the frequency ranges with 10 Hz bandwidth around the resonances and using the RFM, the storage and loss moduli for the adhesive were identified. The results are summarized in Table 3. As it is obvious in Table 3 the results based on RFM and IEM are in nearly close agreement. For better evaluation of the performance of the methods FRF correlation tests have been utilized. FRAC values for each measured FRF and its analytical counterpart after updating are presented in Table 3 for both methods. Also, The ACC between the measured FRFs and those from updated FE model are plotted in Fig. 7. The results show that both methods result in FRFs with high level of correlation in comparison with the experimental FRFs. It is worth considering that in this experiment, dominant modes, far from each other on the frequency axis, made the results of the EMA to be accurate. This is not a general case and as discussed in Section 1, EMA inherently introduces errors and inaccuracies over and above those already present in the measured data. In contrast, in the RFM there is no need to EMA and so, the accuracy of the results is not dependant to the accuracy of EMA.

Table 3: Comparison between the IEM and the RFM around the resonances.

Excitation level (N)	Frequency (Hz)	E' (MPa)	E'' (MPa)	FRAC21	FRAC22	FRAC23	FRAC24
RFM							
3.3	17-27	6.7920	1.4193	0.9868	0.9961	0.9987	0.9971
	394-404	9.5561	1.8196	0.9989	0.9981	0.9918	0.9946
46.2	14-24	5.2407	1.1926	0.9949	0.9872	0.9977	0.9960
	387-397	8.4740	2.1478	0.9997	0.9995	0.9962	0.9975
IEM [a]							
3.3	22.26 Hz	6.9740	1.4827	0.9957	0.9989	0.9973	0.9874
	394.45 Hz	9.6404	1.6085	0.9994	0.9990	0.9912	0.9949
46.2	19.28 Hz	5.1831	1.1757	0.9915	0.9819	0.9957	0.9977
	387.33 Hz	8.7146	2.1234	0.9994	0.9998	0.9972	0.9986

[a] For the IEM the FRAC values have been computed for the frequency ranges same as those for the RFM.

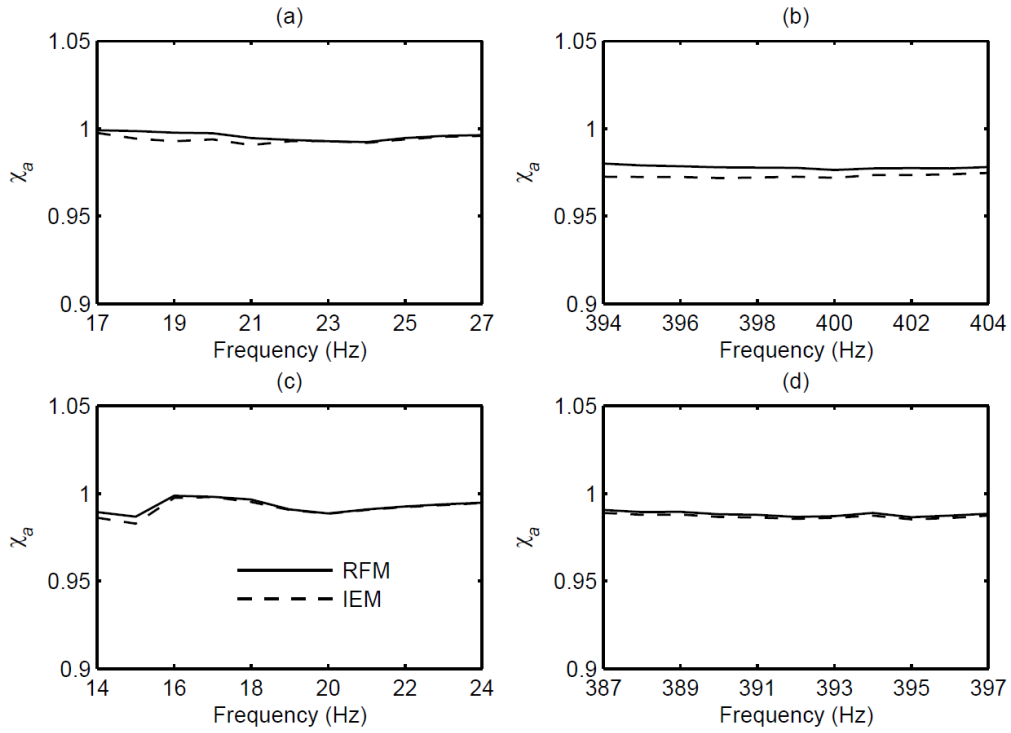

Fig. 7. ACCs between the measured FRFs and those from updated FE model using the RFM around resonances and the IEM.

11. Case study 2: Examining viscoelastic models

In this study five viscoelastic constitutive models, presented in Section 5, will be considered for updating the FE model. According to Fig. 1, it is obvious that the simpler models (1, 2 and 3) are particular cases of more complex models (4 or 5). The justification of separate examination of all of these five models is as follows. First of all, none of the 5 models present the exact model for the adhesive. As such, any of the 5 models, with different level of computational cost, will eventually provide parameters which, when used in FE model, will

provide a degree of correlation with experimental results. It should be noted, however, that, in inverse problems in general and identification process in particular, it is not always the case that a model with more parameters will provide a better representation of the system under identification, as the system behavior might be insensitive to some (redundant) parameters included in the model. This redundancy, or near redundancy, will lead to computational difficulties and problematic convergence and the initial values of the model parameters will have a significant impact on the convergence of the updating process. So all of the 5 models must be check for the sake of the completeness to see which model provides closer correlations with the experimental FRFs. Obviously, if the simpler models result in reasonably correlated FRFs, they will be more preferable than the more complex models because of their simplicity of implementation in the FE modelling.

The Young's modulus of 198 GPa for the beam was used in the FE model as a known value (Section 10). Therefore the only remained unknown parameters in the FE model of bonded beam are parameters of considered viscoelastic model for the adhesive.

First of all, the simplest model, Model 1, is considered to obtain an initial point for sensitivity analysis as well as to gain a first insight for choosing the initial values for the parameters of other models. The initial values of E_0 = 8 MPa and h = 1.5 MPa were chosen. Four measured FRFs of the bonded beam, in the frequency range of 1-500 Hz with the step of 1 Hz were considered for updating process (N_f = 500, N_H = 4 and N_p = 2). After 7 iteration steps the parameters converged to E_0=9.558 MPa and h=1.864 MPa. The results are summarized in Table 4 and the convergence of parameters is shown in Fig. 8.

Table 4: Results of the updating process for the excitation Level 1 using Models 1-5.

	E_0 (MPa)	E_1 (MPa)	η_0 (kPa.sec)	η_1 (kPa.sec)	h (MPa)	$FRAC_{21}$	$FRAC_{22}$	$FRAC_{23}$	$FRAC_{24}$
Model 1									
Initial	8.0000	-	-	-	1.5000	0.8149	0.7090	0.6232	0.6159
Updated	9.5578	-	-	-	1.8643	0.9903	0.9756	0.8806	0.8926
Model 2									
Initial	9.0000	-	0.4000	-	-	0.8693	0.6739	0.1848	0.2184
Updated	9.3684	-	0.7757	-	-	0.9718	0.8981	0.5369	0.5543
Model 3									
Initial	5.0000	4.0000	-	4.0000	-	0.8968	0.7967	0.6710	0.6841
Updated	4.7121	5.5573	-	6.0491	-	0.9866	0.9790	0.8979	0.9106
Model 4									
Initial	6.0000	3.0000	-	3.0000	1.0000				
Updated	6.6700	3.1487	-	4.1810	0.9440	0.9908	0.9863	0.9541	0.9567
Model 5									
Initial	5.5000	3.0000	0.4000	6.0000	-	0.8940	0.8011	0.7233	0.7260
Updated	6.1460	3.4719	0.5502	1.0888	-	0.9933	0.9835	0.9478	0.9516

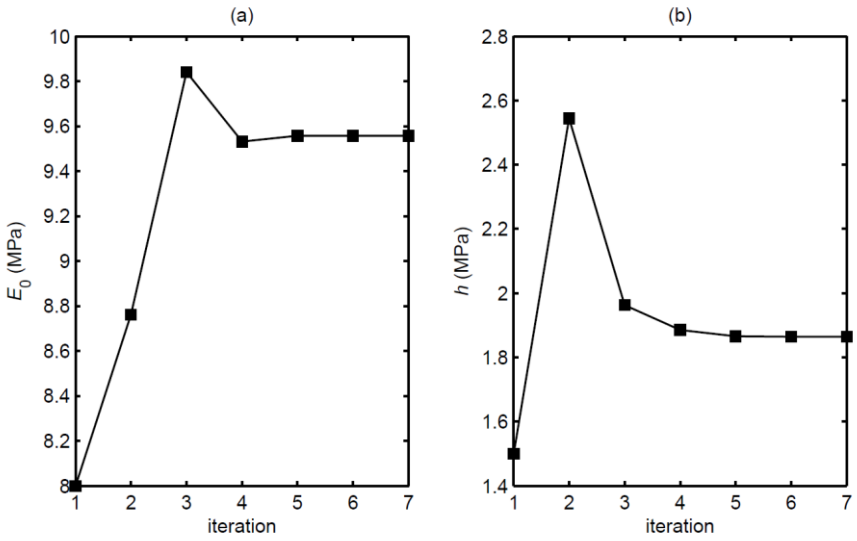

Fig. 8. Convergence of the parameters (a) E_0 and (b) h through iterations in updating process of the FE model considering Model 1 and excitation Level 1.

Using the obtained values for E_0 and h the sensitivities of a typical FRF, H'_{22}, with respect to E' and E'' (or equivalently with respect to E_0 and h) were calculated through Eq. (46)-(47). Since the sensitivities of a FRF are complex functions of frequency, the amplitudes of these functions are presented in Fig. 9. It is obvious that H'_{22} shows significant sensitivity to E' and E'' around resonances.

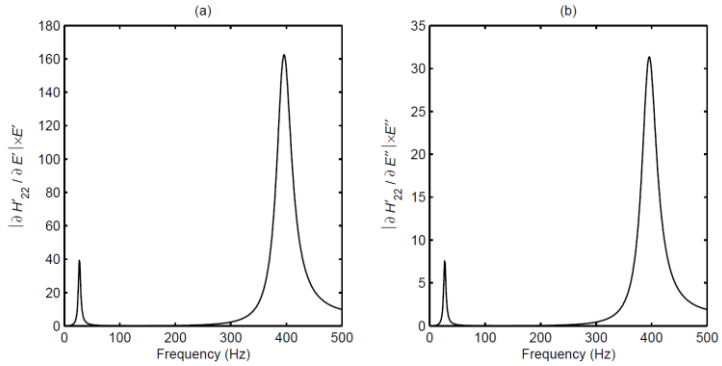

Fig. 9. Normalized absolute value of the sensitivity of H'_{22} with respect to (a) E' and (b) E''.

In continuation, all of the models 2-5 were considered in four different updating efforts separately. The results are summarized in Table 4. To examine the models, FRF correlation tests were applied. For each model, the FRAC values for each measured FRF and its analytical counterpart after updating are presented in Table 4. Also, The SCC and ACC between the measured FRFs and those from updated FE model are illustrated in Fig. 10 for

Model 1, Fig. 11 for Models 2-3 and Fig. 12 for Models 4-5. The identified storage and loss moduli of the adhesive using all of the models are plotted together in Fig. 13 for comparison.

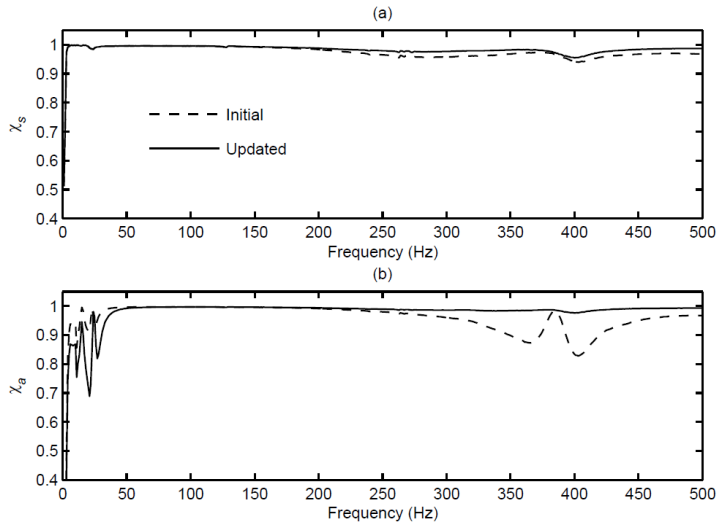

Fig. 10. Correlations between initial and updated FRFs using Model 1 at excitation Level 1.

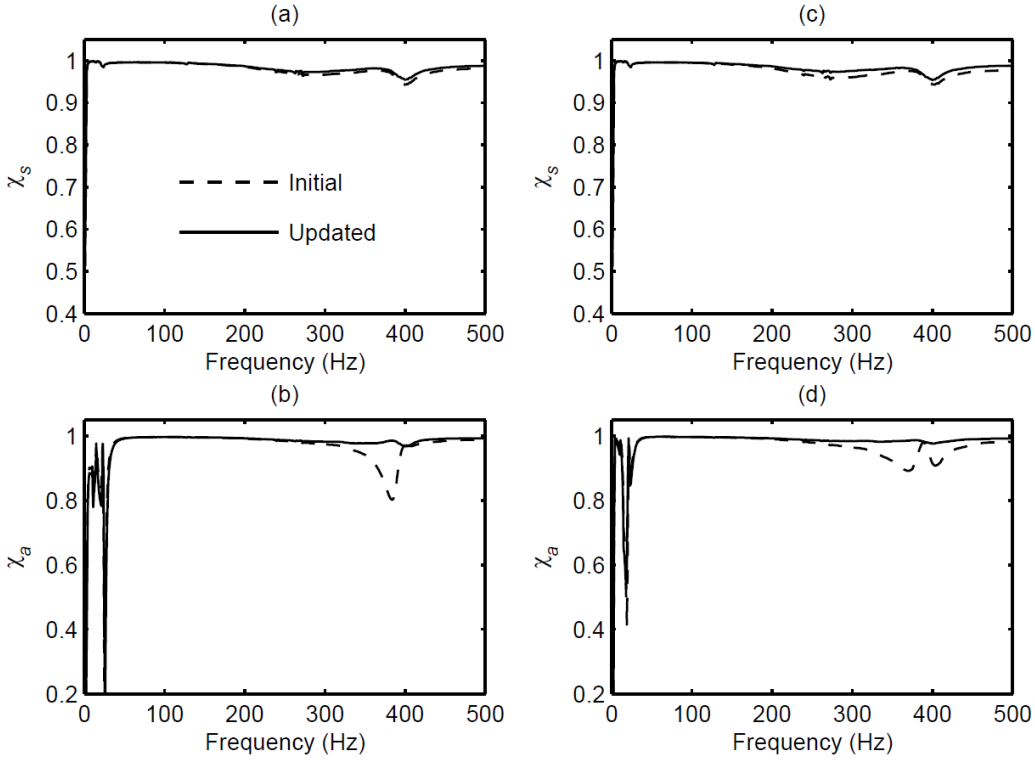

Fig. 11. Correlations between initial and updated FRFs at the excitation Level 1 using Model 2 (a, b) and Model 3 (c, d).

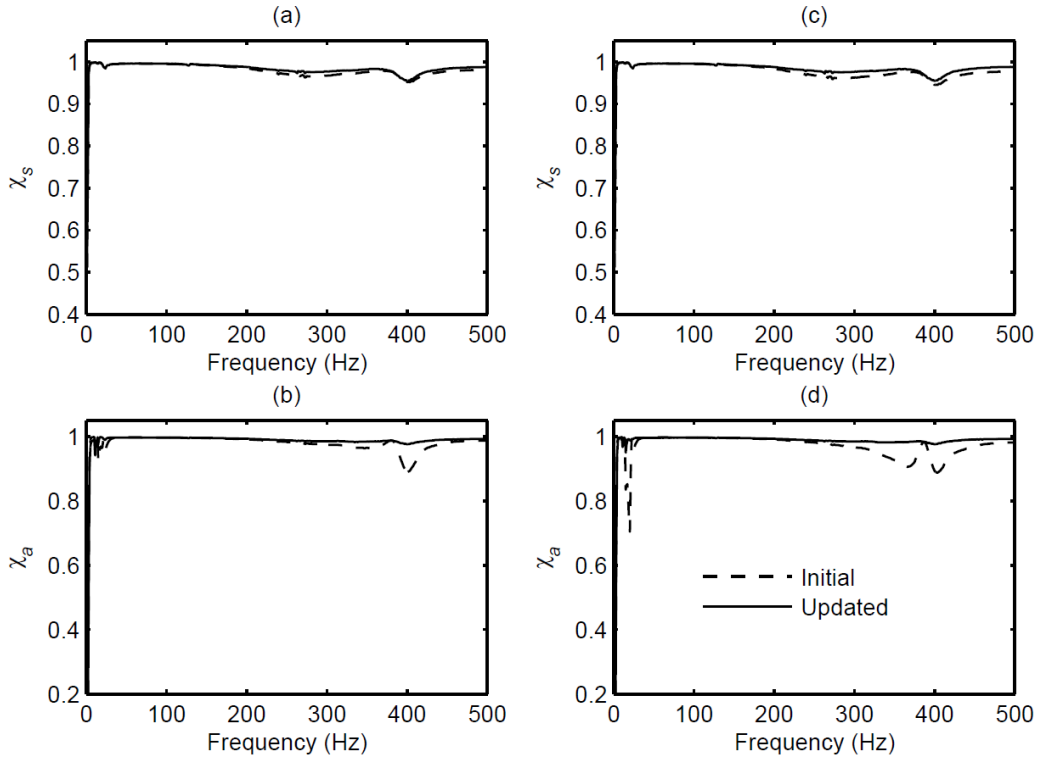

Fig. 12. Correlations between initial and updated FRFs at the excitation Level 1 using Model 4 (a, b) and Model 5 (c, d).

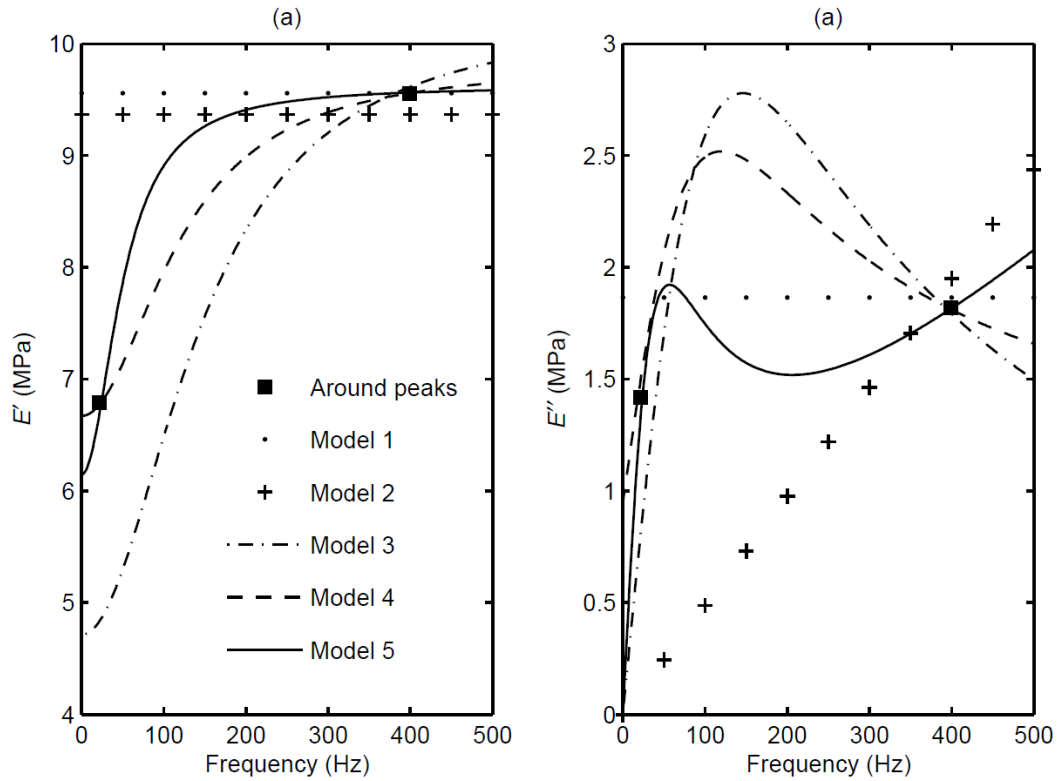

Fig. 13. Comparison between identified (a) storage and (b) loss moduli for the adhesive material at the excitation Level 1.

In the cases of Models 1 and 3 the values of identified E' and E'' are closer to those values obtained for the frequency range around 397 Hz. So, the updated FRFs are more correlated with experimental FRFs in this frequency range and less correlated around 22 Hz. These are obvious in Fig. 10b and Fig. 11d. For Model 2 the value of identified E' is between the values obtained for the frequency range around 22 Hz and 397 Hz. Therefore, less correlation is obtained around these frequencies. This can be seen in Fig. 11b. The best correlation was obtained using Models 4 and 5 and there is no significant discrepancy between the updated FRFs and consequently between results of correlation tests for these two models, as shown in Fig. 12. In Models 4 and 5 cases the values of identified E' and E'' are very close to those values obtained for the frequency range around the peaks. So, the updated FRFs show nearly perfect correlation with experimental FRFs. These are obvious in Fig. 13. The amplitude and phase of measured and updated FRFs for the excitation Level 1, using Model 5 are presented in Fig. 14 and Fig. 15. Nearly the same FRFs were obtained using model 4.

Although the values of FRFs in all of the measured frequency point were exploited in updating process, the values of FRFs around the peaks have significant effect on the updated values of design parameters. This is mainly because of higher sensitivity of FRFs with respect to design parameters around the peaks. Using the measured FRFs one could not conclude that between Model 4 and 5 which one is more accurate and at least one other data points is needed. For example, if any data would be available for static modulus, the best model could be chosen between them.

Different values were reported in the literature for the static (low frequency range) modulus of Sikaflex-252. Some instances are as follows. In the Sikaflex-252 structural adhesive product data sheet [15] the value of shear modulus for the adhesive was reported as 0.7 MPa (approximately). Considering Poisson's ratio of 0.34 the value of Young's modulus becomes 1.876 MPa. Verhoff et al. [17] used the value of 21.7 MPa for the static Young's modulus. Armeanu [18] obtained the Young's modulus as 9.7 MPa according to ASTM D638 on an Instron-4204 universal testing machine with a crosshead speed of 1 mm/min whereas Link and Weiland [19] obtained this value as 6.6 MPa at 21.86 Hz using an eigen frequency based updating method. Huveners et al. [20] carried out a tensile shear test at temperature of 23°C and relative humidity of 60% and obtained the value of shear modulus as 0.5 MPa at the displacement rate of 2.5 mm/min. Considering Poisson's ratio of 0.34, the value of Young's modulus becomes 1.34 MPa. It is obvious that the reported values for the modulus of Sikaflex-252 are very scattered. According to the Table 3, the present method resulted in a

value of 6.974 MPa for the Young's modulus around 22.26 Hz that is in close agreement with the value of 6.6 MPa at 21.86 Hz obtained in [19].

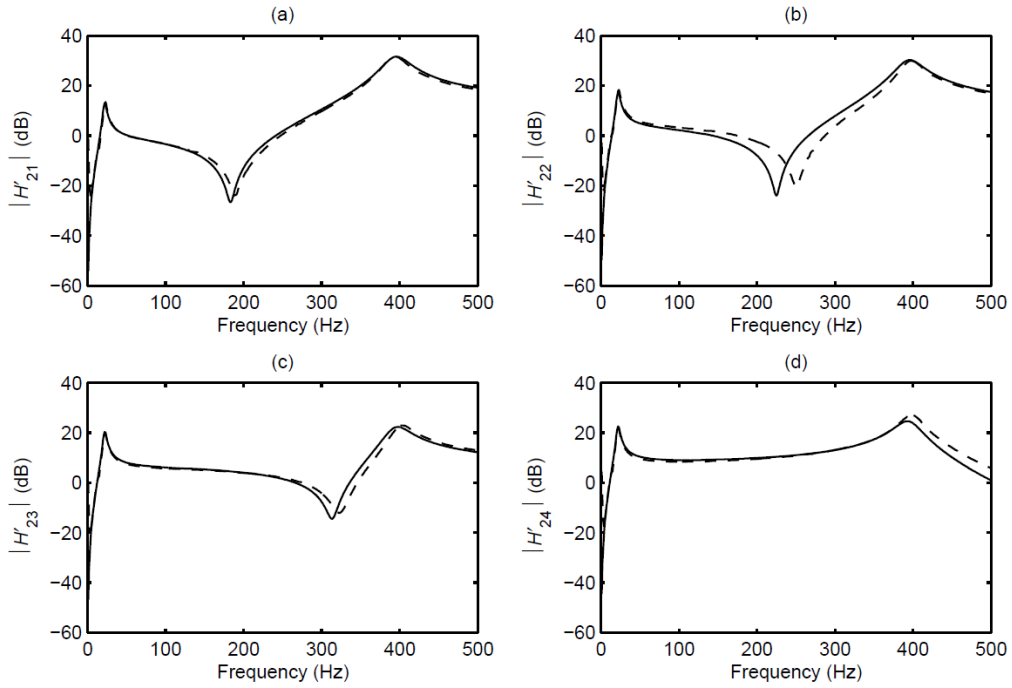

Fig. 14. Amplitude of (dash) measured and (solid) updated FRFs using Model 5 at the excitation Level 1.

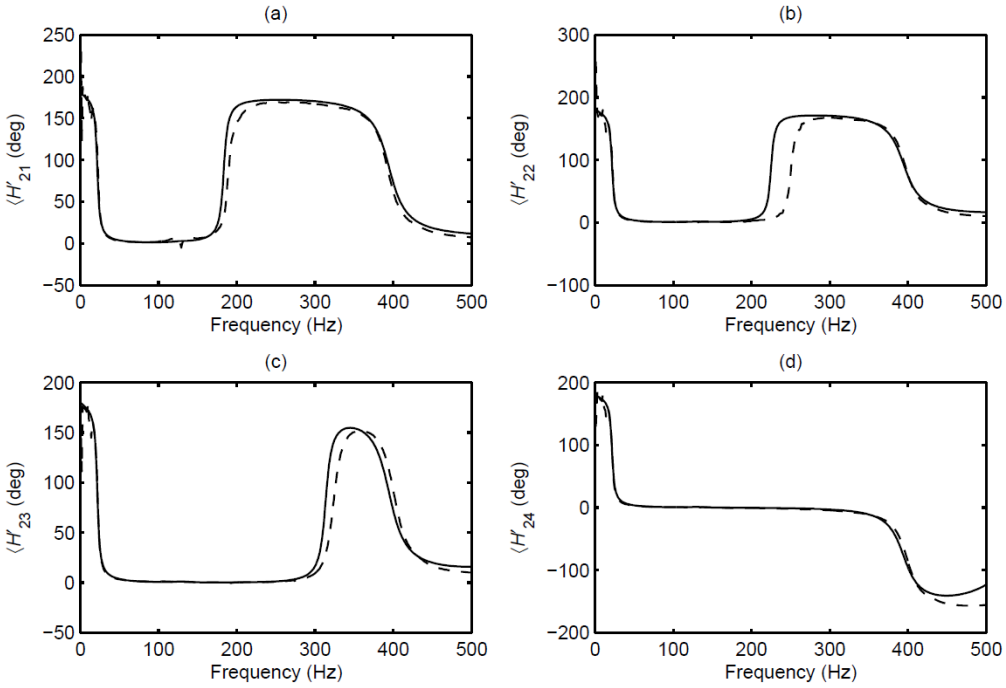

Fig. 15. Phase of (dash) measured and (solid) updated FRFs using Model 5 at the excitation Level 1.

12. Case study 3: Investigation of the effects of excitation level

In this case study, the effects of excitation level on the identified models is investigated. The FE model was updated using Models 4-5 for the excitation Level 2. The results are summarized in Table 5. The amplitude and phase of measured and updated FRFs for the excitation Level 2, using Model 5 are presented in Fig. 16 and Fig. 17 which demonstrate good correlation. Nearly the same FRFs were obtained using model 4. The identified storage and loss moduli in two levels of excitation are plotted in Fig. 18(a, b) for Model 4 and (c, d) for Model 5.

It is obvious from Fig. 18 that, as the level of excitation increased from Level 1 to 2, the storage modulus reduces about 10-23% depending on the frequency. This is not the case for loss modulus. At low frequency band (below 94 Hz for Model 4 and below 45 Hz for Model 5) the loss modulus reduces up to 20%, whereas above these frequency ranges it increases up to 25% depending on the frequency. This observation reveals the nonlinear behavior of the adhesive material which can be identified utilizing the proposed method at different excitation levels.

Table 5: Results of the updating process for the excitation Level 2 using Models 4-5.

	E_0 (MPa)	E_1 (MPa)	η_0 (kPa.sec)	η_1 (kPa.sec)	h (MPa)	$FRAC_{21}$	$FRAC_{22}$	$FRAC_{23}$	$FRAC_{24}$
Model 4	5.1582	3.8978	-	3.8954	0.7703	0.9954	0.9885	0.9647	0.9706
Model 5	4.8691	3.7561	0.5831	8.7038	-	0.9985	0.9841	0.9545	0.9657

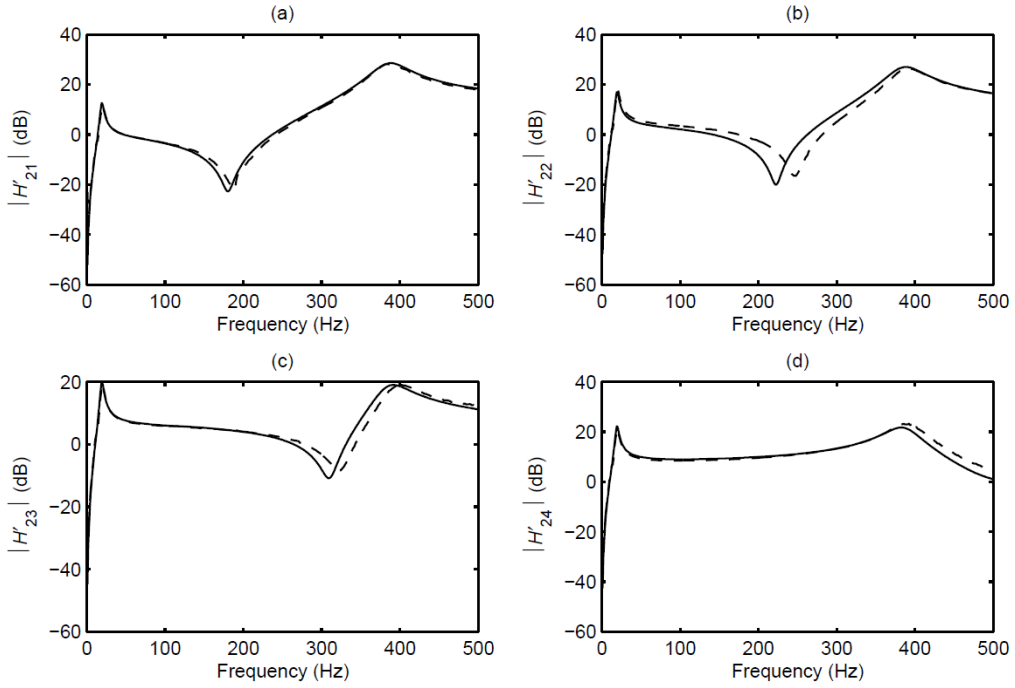

Fig. 16. Amplitude of (dash) measured and (solid) updated FRFs using Model 5 at the excitation Level 2.

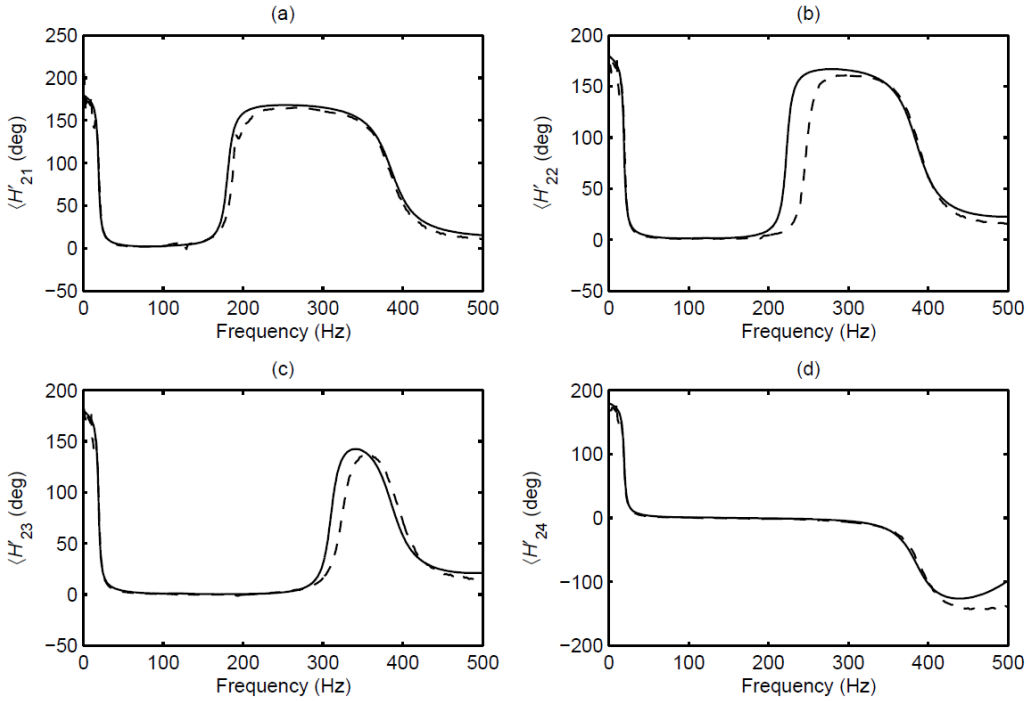

Fig. 17. Phase of (dash) measured and (solid) updated FRFs using Model 5 at the excitation Level 2.

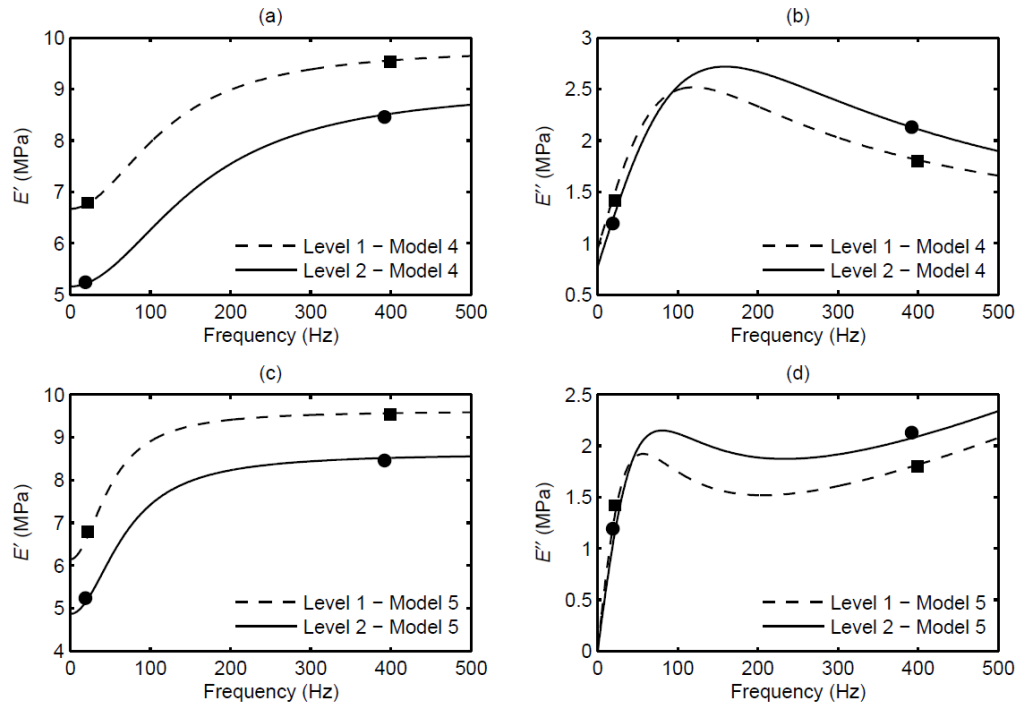

Fig. 18. Identified storage and loss moduli for the adhesive material using (a, b) Model 4 and (c, d) Model 5 at the excitations Level 1-2.

13. Conclusion

The RFM as a FRF-based model updating method was modified for the purpose of identification of parameters in viscoelastic constitutive model. The method was applied to update the FE model of a beam connected to a rigid support via a layer of elastic adhesive using experimentally measured accelerance FRFs. It was shown that the proposed method performs well in FE model updating and consequently in identification of viscoelastic and frequency dependent material properties. The value and frequency of peaks in FRFs have significant effect on the identified parameters. Besides, choosing the appropriate viscoelastic model is crucial in the success of model updating attempt and accuracy of the results. Therefore, the proposed method has the capability to be adopted for identification of the viscoelastic models with the following consideration. Firstly the values of storage and loss modulus must be identified around the resonances. This is similar to that is done usually in modal-based updating method notwithstanding the fact that the FRF-based methods are more preferable as discussed and showed in Section 10. Secondly, a viscoelastic model must be chosen for frequency range of interest with enough flexibility that its storage and loss modulus could intersect those values obtained for frequency bands around the resonances. It was shown that SLS model are not so flexible and a viscous or constant structural damper (stiffness proportional) in parallel with SLS makes it more suitable for the tested adhesive material. Also, it has been shown that, in contrast to the stiffness softening characteristic of the adhesive as the excitation level increases, the loss modulus of the adhesive increases especially at higher frequencies.

References

[1] He X. A review of finite element analysis of adhesively bonded joints. Int J Adhes Adhes 2011;31:248–64. http://dx.doi.org/10.1016/j.ijadhadh.2011.01.006

[2] Najib MF, Nobari AS. Nonlinear viscoelastic constitutive model identification for a polyurethane adhesive in a bonded joint using structural dynamic model updating. Mech Mat 2016;100:72–85. http://dx.doi.org/10.1016/j.mechmat.2016.06.008

[3] García-Barruetabeña J, Cortés F, Abete JM, Fernández P, Lamela MJ, Fernández-Canteli A. Experimental characterization and modelization of the relaxation and complex moduli of a flexible adhesive. Mater Des 2011;32:2783–96. http://dx.doi.org/10.1016/j.matdes.2011.01.005

[4] Maheri MR, Adams RD. Determination of dynamic shear modulus of structural adhesives in thick adherend shear test specimens. Int J Adhes Adhes 2002;22:119-27.

[5] Jahani K, Nobari AS. Identification of dynamic (Young's and shear) moduli of a structural adhesive using modal based direct model updating method. Exp Mech 2008;48:599–611. http://dx.doi.org/10.1007/s11340-008-9131-7

[6] Nobari AS, Jahani K. Identification of damping characteristic of a structural adhesive by extended modal based direct model updating method. Exp Mech 2009;49:785–98. http://dx.doi.org/10.1007/s11340-008-9194-5

[7] Naraghi T, Nobari AS. Identification of the dynamic characteristics of a viscoelastic, nonlinear adhesive joint. J Sound Vibrat 2015;352:92–102. http://dx.doi.org/10.1016/j.jsv.2015.05.010

[8] Lin RM, Ewins DJ. Model Updating Using FRF data. In: Proceedings of the 15th International Seminar on Modal Analysis. Leuven, Belgium, 1990. p. 141–62.

[9] Imregun M, Visser WJ, Ewins DJ. Finite element model updating using frequency response function data – I. Theory and initial investigation. Mech Syst Signal Process 1995;9:187–202.

[10] Visser WJ. Updating structural dynamics models using frequency response data. PhD Thesis, Imperial College London, 1992.

[11] Fox RL, Kapoor MP. Rates of change of eigenvalues and eigenvectors, AIAA J 1968;6(12):2426–29. http://dx.doi.org/10.2514/3.5008

[12] Heylen W, Lammens S. FRAC: a consistent way of comparing frequency response functions. In: Proceedings of International Conference on Identification in Engineering Systems. Swansea, Wales, 1996. p. 48–57.

[13] Grafe H. Model updating of large structural dynamics models using measured response functions. PhD Thesis, Imperial College London, 1998.

[14] Kashani H, Nobari AS. Identification of dynamic characteristics of nonlinear joint based on the optimum equivalent linear frequency response function. J Sound Vibrat 2010;329:1460–79. http://dx.doi.org/10.1016/j.jsv.2009.11.007

[15] Sikaflex-252, Product Data Sheet, Version 1 (02/2009), (http://zaf.sika.com).

[16] Ewins DJ. Modal Testing, Theory, Practice, and Application. 2nd ed. Hertfordshire: Research Studies Press; 2000.

[17] Verhoff J, Ramani K, Blank N, Rosenberg S. Moisture durability of four moisture cure urethane adhesives. J Adhes Sci Technol 2002;16(4):373–93. http://dx.doi.org/10.1163/156856102760067172

[18] Armeanu LE. Analysis of bonded joints for small craft and marine applications. Master of Engineering Thesis, University of Waikato, Hamilton, New Zealand, 2010.

[19] Link M, Weiland M. Damage identification by computational model updating. In: Proceedings of the 9th Biennial ASME Conference on Engineering Systems Design and Analysis. Haifa, Israel, 2008. p. 683-93. http://dx.doi.org/10.1115/ESDA2008-59349

[20] Huveners EMP, Van Herwijnen F, Soetens F, Hofmeyer H. Mechanical shear properties of adhesives. In: Proceedings of the 10th International Conference on Architectural and Automotive Glass. Tampere, Finland, 2007. p. 367-70.